Morphological stability of spherical particles - Extension of the Mullins-Sekerka criteria to multi-component alloys under a non-stationary diffusive regime

Gildas Guillemot*, Charles-André Gandin

MINES ParisTech, PSL Research University, CEMEF UMR CNRS 7635, CS10207, 06904 Sophia Antipolis, France

Abstract

An extension of the pioneer work by Mullins and Sekerka is proposed to analyze the stability conditions of a spherical particle growing in a matrix phase. The present model describes the onset of instabilities in unsteady growth regime for multi-components alloys with cross-diffusion of chemical species. The developments are based on the decomposition of initial perturbations in spherical harmonics to determine their time evolution. Expressions for the threshold particle radii associated to the limits for absolute and relative stability criteria are derived. They depend on the degree of the spherical harmonic functions, the growth parameter for a sphere (proportional to the interface velocity times the square root of time) and the eigenvalues of the diffusion matrix. Large effect of the interface velocity on the stability domains is demonstrated considering the time-dependent solutions. Comparisons are provided regarding more recent solutions proposed in the literature. Similar evolution is only observed for slow regimes. An application for solidification of a ternary alloy is finally given.

Keywords: Stability analysis, Multicomponent alloy, Unsteady growth, Cross diffusion, Solidification

1. Introduction

Morphological stability of spherical particles formed by solute diffusion in a matrix phase is of paramount interest in materials science. Common situations are the growth of solid grains in its surrounding liquid during solidification processing or the precipitation of intermetallic particles in its solid solution during heat treatment [1, 2, 3]. Depending from the applying conditions, the particles may evolve with spherical (or globular) shape if stability is preserved, cauliflower and dendritic shape otherwise. This may lead to various microstructures, redistribution of solute species, sequences of phase transformations and material properties [4]. The pioneering work by Mullins and Sekerka published in 1963 introduces the stability analysis of a spherical particle under the assumption of a steady growth regime for a binary alloy [5]. Hence, the diffusion field in the matrix surrounding the particle is given by the Laplace equation for a single solute specie. The interface curvature and its associated capillary effect are also included. Two criteria are derived that express the conditions for a particle of radius R to develop an instability of amplitude δ at its interface with the matrix. The first criterion is referred to as *absolute stability* as it simply states that instabilities develop with the perturbations, $\dot{\delta} > 0$. This condition is reached above a threshold value of the radius, R_a. The second criterion compares the development of the perturbation, $\dot{\delta}/\delta$, with that of the radius, $\dot{R}/R$. It is referred to as the *relative stability* criterion and defines another threshold value of the particle radius, R_r. Using the minimum possible degree of the spherical harmonic for both criteria, Mullins and Sekerka show that $R_a/R^* = 7$ and $R_r/R^* = 21$ where R^* is the critical nucleation radius.

Few additional works are reported in the literature in order to overcome some of the simplifying assumptions. Wey and Estrin were among the first to mention the limit associated to the use of the Laplace equation, i.e. the neglecting of the temporal variation in solute mass conservation equation [6, 7]. From velocity dependent criteria, they retrieve similar results as Mullins and Sekerka in the limit of low velocity. The effect of the kinetics undercooling is available since the work of Wang et al. [8, 9, 10]. More recently, Colin and Voorhees [11] propose a stability analysis under a steady growth regime for a ternary alloy, also considering the kinetics undercooling. However, cross diffusion effects are not considered and comparisons with Mullins and Sekerka criteria are only proposed when the kinetics effect vanishes. They show that a third element only modifies the critical nucleation radius while the same expressions of the criteria apply. The study by Diepers and Karma [12] on the globular-to-dendritic transition using phase field simulations also demonstrates the existence of a scaling law with the critical nucleation radius, the

*Corresponding author

Email address: Gildas.Guillemot@mines-paristech.fr (Gildas Guillemot)

cooling rate and the alloy properties.

The present work extends the previous criteria of literature to multi-component alloys including cross diffusion effects. Unsteady growth regime is accounted for, the initial configuration being a particle of critical nucleation size formed in a supersaturated matrix with uniform composition. Thus, the criteria cover the all range from very slow to very rapid growth regimes. We first present the mathematical model with its hypotheses and derive general expressions of threshold radii associated to the stability criteria. These solutions are compared to previous literature [5, 7, 11]. Applications is finally given to highlight the interest of the new stability criteria by illustrating the role of cross diffusion for the growth stability of a sphere in a ternary metallic alloy as a function of the initial supersaturation.

2. Mathematical Model

2.1. Unsteady growth regime

An isolated particle of thermodynamic phase p is placed in an infinite matrix domain of phase m as schematized in Fig. 1. The domain associated to the particle and to the matrix are respectively named Ω^p and Ω^m. The particle geometry is assumed one-dimensional (1D) with time-dependent radius R as long as the spherical symmetry is preserved. The interface between domains located at distance R is defined as Ω^{pm}. The growing velocity of the interface, $\mathbf{v}$, is directed along the radial unit vector $\mathbf{u}_r$. The material is a multi-component alloy made of the solvent plus N added solute species. The molar composition at large distance is supposed to remain constant for any solute specie i, equal to $X_i^{m,\infty}$ ($i \in \{1, N\}$). This set of N compositions defines the vector of the far field composition of the solute species, $\mathbf{X}^{m,\infty}$. Compositions in the particle and the matrix at the interface are respectively denoted by $X_{i,\kappa}^{pm}$ and $X_{i,\kappa}^{mp}$ for any solute specie i and interfacial curvature κ. The particle and matrix phases have similar constant molar volume equal to V_m. In addition, all the system evolves at a fixed temperature T. The molar composition for any solute specie i satisfies the mass conservation equation in both phases. Considering the composition vector of the solute species in phase $\varphi \in \{p, m\}$, $\mathbf{X}^\varphi$, the solute mass conservation equation writes:

$$\mathbf{D}^\varphi \cdot \nabla^2 \mathbf{X}^\varphi = \frac{\partial \mathbf{X}^\varphi}{\partial t} \tag{1}$$

where $\mathbf{D}^\varphi$ is the diffusion matrix in the φ phase, each D_{ij}^φ term being assumed constant. Consequently, $-D_{ij}^\varphi \boldsymbol{\nabla} X_j^\varphi$ is the contribution of the composition gradient of elements j to the diffusion flux of element i in phase φ. Fig. 1 schematizes the non monotonous composition profile that could be observed at a given time for two elements, 1 and 2, induced by the cross diffusion phenomenon.

Growth and dissolution proceed due to the solute fluxes created at the Ω^{pm} interface in both the particle phase and the matrix phase. The solute balance at the Ω^{pm} interface relates the interfacial compositions, $X_{i,\kappa}^{pm}$ and $X_{i,\kappa}^{mp}$ of any element $i \in \{1, N\}$ to the solute fluxes:

$$\begin{aligned} &\left(X_{i,\kappa}^{mp} - X_{i,\kappa}^{pm}\right) \mathbf{v} \cdot \mathbf{n} = \\ &\sum_{j=1}^{N} -D_{ij}^m \nabla^{mp} X_j^m \cdot \mathbf{n} - \sum_{j=1}^{N} -D_{ij}^p \nabla^{pm} X_j^p \cdot \mathbf{n} \end{aligned} \tag{2}$$

where $\nabla^{mp} X_j^m$ and $\nabla^{pm} X_j^p$ are respectively the composition gradient of solute specie j in the matrix m and in the particle p at the Ω^{pm} interface of local normal $\mathbf{n}$ and curvature κ. The interfacial composition vectors in the matrix and in the particle, respectively $\mathbf{X}_\kappa^{mp}$ and $\mathbf{X}_\kappa^{pm}$, are defined as the set of N solute compositions at the Ω^{pm} interface corresponding to $X_{i,\kappa}^{mp}$ and $X_{i,\kappa}^{pm}$ with $i \in \{1, N\}$. These compositions are assumed in thermodynamic equilibrium at any temperature T defined by the following relations:

$$\mathbf{X}_\kappa^{mp} = \mathrm{F}^{mp}(\mathbf{X}_0^{mp}, T, \kappa) \tag{3}$$

$$\mathbf{X}_\kappa^{pm} = \mathrm{F}^{pm}(\mathbf{X}_0^{mp}, T, \kappa) \tag{4}$$

In the absence of curvature (for a flat interface with $\kappa = 0$), function F^{mp} essentially locates the hypersurface of the matrix composition in equilibrium with the particle, $\mathbf{X}_0^{mp}$, at any temperature T, e.g. the *liquidus* or the *solvus* of a phase diagram. The corresponding vector of the equilibrium composition in the particle is $\mathbf{X}_0^{pm}$ given by function F^{pm}, i.e. providing with the equilibrium *tie lines* of the phase diagram. So Eqs (3) and (4) extend the description of the phase diagram by adding the Gibbs-Thomson effect due to curvature κ.

The authors previously investigated the development of a spherical particle in a multicomponent alloy with cross diffusion and under unsteady growth regime [1, 2]. They demonstrated that the previous set of equations has a single solution when neglecting the effect of curvature and the solute flux in the particle. Assuming a very small initial radius of the particle at time $t = 0$ s, the unsteady growth regime is observed with time dependent solute profile in the matrix. The radius evolves with the following simple relation:

$$R = \lambda \sqrt{t} \tag{5}$$

where the growth parameter λ is defined as the solution of the set of Eqs (3) and (4) plus the following relation:

$$\boldsymbol{\Delta} \mathbf{X}_0^{mp} = \boldsymbol{\Gamma}(\lambda) \boldsymbol{\Delta} \mathbf{X}_0^m \tag{6}$$

where $\boldsymbol{\Delta} \mathbf{X}_0^{mp}$ = $\mathbf{X}_0^{mp}$ - $\mathbf{X}_0^{pm}$ is the vector associated to the composition jump at the interface between the particle and the matrix and $\boldsymbol{\Delta} \mathbf{X}_0^m$ = $\mathbf{X}_0^{mp}$ - $\mathbf{X}^{m,\infty}$ is the difference between the interfacial composition in the matrix and the composition at a very large distance, assumed

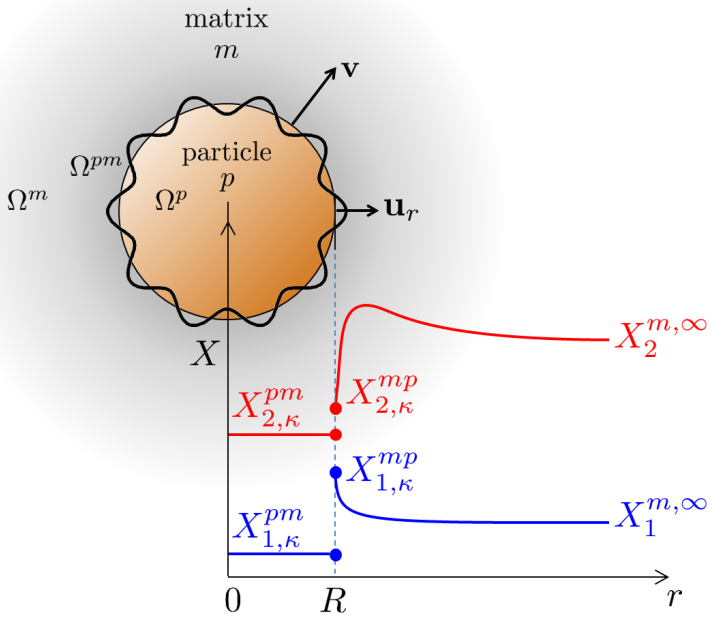

Figure 1: Illustration of (orange) a particle phase, p, embedded in (grey) a matrix phase, m, at a given temperature, T, together with schematized molar composition profiles for (blue) component 1 and (red) component 2 in both domains Ω^p and Ω^m. The interface separating the two domains, Ω^{pm}, is schematized by a black line for both (thin) a stable spherical particle shape and (thick) a perturbed form at the onset of instability.

fixed as already stated before. The $\mathbf{\Gamma}(\lambda)$ matrix is the set of Γ_{ij} elements ($(i,j) \in \{1,N\}^2$) defined as:

$$\Gamma_{ij} = \sum_{k=1}^{N} U_{ik} U_{kj}^{-1} G\left(\frac{\lambda^2}{B_k}\right) \tag{7}$$

where B_k is the k-eigenvalue of the diffusion matrix $\mathbf{D}^m$. Similarly, the vector $\mathbf{U_k}$ ($k \in \{1,N\}$) of components U_{ik} ($i \in \{1,N\}$) is the k-eigenvector associated to the B_k value. The $\mathbf{U}$ matrix is defined by the set of $\mathbf{U_k}$ vectors and associated to the transfer matrix. The G function is mathematically defined as:

$$G(x) = \frac{2}{x\left(1 - \frac{\sqrt{\pi}}{2}\sqrt{x}\,\mathrm{e}^{x/4}\,\mathrm{erfc}\left(\frac{\sqrt{x}}{2}\right)\right)} \tag{8}$$

The set of non-linear Eqs (3), (4) and (6) and its resolution provide the conditions for the growth of a spherical particle. It also defines the particle and matrix compositions at the Ω^{pm} interface, X_0^{pm} and X_0^{mp}, as well as the λ growth parameter value associated to the interface evolution under unsteady growth. If the Gibbs-Thomson effect is neglected, constant values are obtained from such resolution [1, 2].

2.2. Instabilities development

The aim of the present study is to investigate the development of instabilities occurring in growing conditions previously described. We may consider infinitesimal instabilities developed at the Ω^{pm} interface as schematized by the thick black contour in Fig. 1. Following the approach by Mullins and Sekerka [5], any perturbation of the spherical shape with average radius R may be decomposed in a set of spherical harmonics $Y_{(l)}^{(m)}(\theta,\varphi)$ with specific amplitude δ. Consequently, the local radius in spherical coordinates associated to such perturbation is defined as:

$$r = R + \delta\, Y_{(l)}^{(m)}(\theta,\varphi) \tag{9}$$

with

$$Y_{(l)}^{(m)}(\theta,\varphi) = \sqrt{\frac{2\,l+1}{4\,\pi}\frac{(l-m)!}{(l+m)!}}\, P_{(l)}^{(m)}(\cos(\theta))\,\mathrm{e}^{im\varphi} \tag{10}$$

where R and δ are time dependent variables, $Y_{(l)}^{(m)}(\theta,\varphi)$ is the spherical harmonic function of degree l and order m that only depends on the interface position given by the polar angle, θ, and the azimuthal angle, φ, defined by the spherical coordinate system and $P_{(l)}^{(m)}$ is the associated Legendre polynomial. The curvature, κ, associated to the interfacial perturbation writes [5]:

$$\kappa = \frac{2}{R} + (l+2)(l-1)\frac{\delta\, Y_{(l)}^{(m)}}{R^2} \tag{11}$$

where the dependence (θ, φ) of the spherical harmonic function is omitted for simplicity.
In order to compute the time evolution of the product $\delta\ Y_{(l)}^{(m)}$ at the onset of a perturbation, we first have to estimate the associated composition field. Neglecting the solute flux in the particle, only the matrix phase is considered [5]. Regarding the solute conservation equation (Eq. (1)) with $\varphi = m$, the $\mathbf{D}^m$ matrix can be replaced by its diagonalized expression $\mathbf{U} \cdot \mathbf{B}^m \cdot \mathbf{U^{-1}}$. The constant variable $\mathbf{B}^m$ refers to the diagonal matrix based on the B_i^m eigenvalues of $\mathbf{D}^m$. The constant variable $\mathbf{U}$ refers to the transfer matrix based on the eigenvectors $\mathbf{U}_{\cdot}$ of $\mathbf{D}^m$. The solute conservation equation writes:

$$\mathbf{B}^m \cdot \nabla^2 \widetilde{\mathbf{X}}^m = \frac{\partial \widetilde{\mathbf{X}}^m}{\partial t} \tag{12}$$

where $\widetilde{\mathbf{X}}^m$ is the intermediate composition vector variable $\mathbf{U^{-1}} \cdot \mathbf{X}^m$. Eq. (12) is a set of N independent equations $B_i^m\ \nabla^2 \widetilde{X}_i^m = \partial \widetilde{X}_i^m / \partial t\ (i \in \{1, N\})$ to be solved with initial and boundary conditions associated to the solute field on the perturbed interface.

2.2.1. Solute composition field

The general solution can be derived considering three particular solutions. The first solution is given by the composition at infinity or far field composition, $\widetilde{X}_i^{m,\infty}$, assumed constant and depending from $X_i^{m,\infty}$. The second solution corresponds to the fundamental solution without perturbation (i.e., $r = R$ and $\delta = 0$) associated to the constant function $Y_{(0)}^{(0)}$. This latter has been previously derived by the authors [1, 2]:

$$\widetilde{X}_{i,(0)}^m = \zeta_{i,(0)}\ F_{(0)}\left(\frac{r^2}{B_i^m\ t}\right) Y_{(0)}^{(0)} \tag{13}$$

where $\zeta_{i,(0)}$ is a constant value and function $F_{(0)}$ is given by:

$$F_{(0)}(x) = 4\ \frac{\mathrm{e}^{-x/4}}{\sqrt{x}} - 2\ \sqrt{\pi}\ \mathrm{erfc}\left(\frac{\sqrt{x}}{2}\right) \tag{14}$$

As demonstrated in [1, 2], the G function (Eq. 8) is no more than $-4\ F'_{(0)}/F_{(0)}$ where $F'_{(0)}$ is the derivative of the $F_{(0)}$ function. The third solution is associated to a single perturbation. In the space of the diagonal system Eq. (12) can be rewritten:

$$B_i^m \left(\frac{1}{r}\frac{\partial^2\left(r\widetilde{X}_i^m\right)}{\partial r^2} + \frac{1}{r^2}\Lambda \widetilde{X}_i^m\right) = \frac{\partial \widetilde{X}_i^m}{\partial t} \tag{15}$$

where the Laplace operator ∇^2 in Eq. (12) has been decomposed in radial and angular parts. The angular part, Λ, is defined hereafter:

$$\Lambda = \frac{1}{\sin(\theta)}\frac{\partial}{\partial \theta}\left(\sin(\theta)\frac{\partial}{\partial \theta}\right) + \frac{1}{\sin^2(\theta)}\frac{\partial^2}{\partial \varphi^2} \tag{16}$$

We may consequently consider a mathematical general form of solution depending from the harmonic function: $\widetilde{X}_{i,(l)}^m(r, \theta, \varphi, t) = F_{i,(l)}(r, t)\, \delta\ Y_{(l)}^{(m)}(\theta, \varphi)$, where $F_{i,(l)}$ is an unknown function to be determined. The angular part has $Y_{(l)}^{(m)}$ as eigenfunctions with associated eigenvalues $-l(l+1)$ (i.e. $\Lambda Y_{(l)}^{(m)} = -l\ (l+1)\ Y_{(l)}^{(m)}$) [13]. Consequently, function $F_{i,(l)}(r, t)$ corresponds to the solution of the differential equation:

$$B_i^m \left(\frac{1}{r}\frac{\partial^2\left(rF_{i,(l)}\right)}{\partial r^2} - l(l+1)\frac{F_{i,(l)}}{r^2}\right) = \frac{\partial F_{i,(l)}}{\partial t} \tag{17}$$

After the change of variable $\xi_i = r^2/(B_i^m\ t)$ [14], we look for the solution $\widetilde{F}_{(l)}(\xi_i)$ of equation:

$$4\ \xi_i^2\ \frac{\partial^2 \widetilde{F}_{(l)}}{\partial \xi_i^2} + (6\xi_i + \xi_i^2)\frac{\partial \widetilde{F}_{(l)}}{\partial \xi_i} - l(l+1)\widetilde{F}_{(l)} = 0 \tag{18}$$

The general form of the $\widetilde{X}_{i,(l)}^m$ composition field can then be expressed as a function of $\widetilde{F}_{(l)} = \zeta_{i,(l)}\ F_{(l)}$:

$$\widetilde{X}_{i,(l)}^m = \zeta_{i,(l)}\ F_{(l)}\left(\frac{r^2}{B_i^m\ t}\right)\ \delta\ Y_{(l)}^{(m)} \tag{19}$$

where $\zeta_{i,(l)}$ is a constant value and function $F_{(l)}$ is the single solution of Eq. (18) that does not diverge for infinite argument values:

$$F_{(l)}(x) = \mathrm{e}^{-x/4}\, x^{l/2}\, U\left[\frac{3+l}{2}, \frac{3}{2} + l, \frac{x}{4}\right] \tag{20}$$

and U is defined as the 3 arguments confluent hypergeometric or Tricomi's function [13]. It should be pointed out that this function is an extension of the previous expression (Eq. (14)) as $F_{(l=0)} = F_{(0)}$ with $U\,[3/2, 3/2, x/4]$. The general solution of Eq. (12) is thus the summation of the three previous solutions:

$$\begin{aligned}\widetilde{X}_i^m &= \widetilde{X}_i^{m,\infty} \\ &+ \zeta_{i,(0)}\ F_{(0)}\left(\frac{r^2}{B_i^m\ t}\right) Y_{(0)}^{(0)} \\ &+ \zeta_{i,(l)}\ F_{(l)}\left(\frac{r^2}{B_i^m\ t}\right)\ \delta\ Y_{(l)}^{(m)}\end{aligned} \tag{21}$$

The 2 N variables $\zeta_{i,(0)}$ and $\zeta_{i,(l)}$ are unknown values to be determined in order to access the full composition field. We can express the components of the real composition vector from Eq. (21):

$$\begin{aligned}X_i^m = X_i^{m,\infty} + \\ \sum_{j=1}^{N} U_{ij}\left(\zeta_{j,(0)}\ F_{(0)}\left(\frac{r^2}{B_j^m\ t}\right) Y_{(0)}^{(0)}\right. \\ \left. + \zeta_{j,(l)}\ F_{(l)}\left(\frac{r^2}{B_j^m\ t}\right)\ \delta\ Y_{(l)}^{(m)}\right)\end{aligned} \tag{22}$$

At the perturbed interface, $r = R + \delta\ Y_{(l)}^{(m)}$, it must verify $X_{i,\kappa}^{mp} = X_i^m(R + \delta\ Y_{(l)}^{(m)})$:

$$\begin{aligned} X_{i,\kappa}^{mp} &= X_i^{m,\infty} + \\ \sum_{j=1}^{N} U_{ij} \Bigg(& \zeta_{j,(0)}\ F_{(0)} \left(\frac{\left(R + \delta\ Y_{(l)}^{(m)}\right)^2}{B_j^m\ t} \right) Y_{(0)}^{(0)} \\ & + \zeta_{j,(l)}\ F_{(l)} \left(\frac{\left(R + \delta\ Y_{(l)}^{(m)}\right)^2}{B_j^m\ t} \right)\ \delta\ Y_{(l)}^{(m)} \Bigg) \end{aligned} \tag{23}$$

At the onset of the perturbation, the growth regime for radius R has not changed much compared to the one before the occurrence of an instability. Consequently, the same expression, $R = \lambda\sqrt{t}$ [1] could still be applied. After developments and neglecting second order terms we obtain:

$$\begin{aligned} X_{i,\kappa}^{mp} &= X_i^{m,\infty} + \\ \sum_{j=1}^{N} U_{ij} \Bigg(& \zeta_{j,(0)}\ F_{(0)}\,(u_j)\, Y_{(0)}^{(0)} + \zeta_{j,(l)}\ F_{(l)}\,(u_j)\,\delta\ Y_{(l)}^{(m)} \\ & + \frac{2\ u_j\ \delta\ Y_{(l)}^{(m)}}{R} \zeta_{j,(0)}\ F'_{(0)}\,(u_j)\, Y_{(0)}^{(0)} \Bigg) \end{aligned} \tag{24}$$

where $u_j = \lambda^2 / B_j^m$ is a dimensionless growth parameter for solute j.

2.2.2. Curvature undercooling

The curvature undercooling, ΔT_κ, is induced by the local radius of curvature at the Ω^{pm} interface. Its value is proportional to the deviation of the interface compositions with the effect of curvature, ($X_{i,\kappa}^{mp}$ - $X_{i,0}^{mp}$), for all solute species i ($i \in \{1, N\}$). Considering a linearized approximation of Eq. (3), i.e. constant slopes of the phase diagram, m_i, for any solute specie i, one can write

$$\Delta T_\kappa = \sum_{i=1}^{N} m_i \left(X_{i,\kappa}^{mp} - X_{i,0}^{mp} \right) = \kappa\ \Gamma \tag{25}$$

where Γ is the Gibbs-Thomson coefficient and κ is the local curvature.
We follow the methodology proposed by Mullins and Sekerka [5] to define the nucleation radius, R^*, considering that its formation takes place at composition $X_{i,\kappa}^{mp} = X_i^{m,\infty}$. Neglecting instabilities effect in Eq. (11), Eq. (25) becomes:

$$R^* = -\frac{2\ \Gamma}{\sum\limits_{i=1}^{N} m_i\ \Delta X_{i,0}^m} \tag{26}$$

Regarding Eq. (24), (25) and (11), we can estimate the curvature undercooling as:

$$\begin{aligned} \Delta T_\kappa &= \sum_{i=1}^{N} m_i \Bigg[X_i^{m,\infty} - X_{i,0}^{mp} \\ &\quad + \sum_{j=1}^{N} U_{ij} \Bigg(\zeta_{j,(0)}\ F_{(0)}\,(u_j)\, Y_{(0)}^{(0)} + \zeta_{j,(l)}\ F_{(l)}\,(u_j)\,\delta\ Y_{(l)}^{(m)} \\ &\quad + \frac{2\ u_j\ \delta\ Y_{(l)}^{(m)}}{R} \zeta_{j,(0)}\ F'_{(0)}\,(u_j)\, Y_{(0)}^{(0)} \Bigg) \Bigg] \\ &= \frac{2}{R}\Gamma + (l+2)(l-1)\frac{\delta\ Y_{(l)}^{(m)}(\theta,\varphi)}{R^2}\Gamma \end{aligned} \tag{27}$$

In Eq. (27), separation of the terms of first order associated to the main radius, R, and of the second order associated to instability, $\delta\ Y_{(l)}^{(m)}$, leads to the following two relations:

$$\begin{aligned} & \sum_{i=1}^{N} m_i \sum_{j=1}^{N} U_{ij}\ \zeta_{j,(0)}\ F_{(0)}\,(u_j)\, Y_{(0)}^{(0)} - \sum_{i=1}^{N} m_i\ \Delta X_{i,0}^m \\ & = \frac{2}{R}\Gamma \end{aligned} \tag{28}$$

$$\begin{aligned} & \sum_{i=1}^{N} m_i \sum_{j=1}^{N} U_{ij} \left(\frac{2u_j}{R}\ \zeta_{j,(0)}\ F'_{(0)}\,(u_j)\, Y_{(0)}^{(0)} + \zeta_{j,(l)}\ F_{(l)}\,(u_j) \right) \\ & = \frac{\Gamma}{R^2}(l+2)(l-1) \end{aligned} \tag{29}$$

2.2.3. Interfacial composition balance

The composition field, both the terms of first order, Eq. (28), and second order Eq. (29), is associated to the unknown parameters $\zeta_{j,(0)}$ and $\zeta_{j,(l)}$ initially introduced in the general form of solution Eq. (21). Assuming that the diffusion flux in the solid phase can be neglected, the solute balance at the Ω^{pm} interface, Eq. (2) now rewrites:

$$\begin{aligned} & \left(X_{i,\kappa}^{mp} - X_{i,\kappa}^{pm} \right) v = \\ & - \sum_{k=1}^{N} D_{ik}^m \sum_{j=1}^{N} U_{kj} \frac{2\ r}{B_j^m\ t} \Bigg(\zeta_{j,(0)}\ F'_{(0)} \left(\frac{r^2}{B_j^m t} \right) Y_{(0)}^{(0)} \\ & + \ \zeta_{j,(l)}\ F'_{(l)} \left(\frac{r^2}{B_j^m t} \right) \delta\ Y_{(l)}^{(m)} \Bigg)_{|r=R\ +\ \delta\ Y_{(l)}^{(m)}} \end{aligned} \tag{30}$$

where $v = \mathbf{v} \cdot \mathbf{u}_r$ stands for the velocity component at the Ω^{pm} interface in the radial direction $\mathbf{u}_r$. This equation only accounts for the radial projection of the composition gradient. It is thus only valid at the onset of the instability

when $\mathbf{n} = \mathbf{u}_r$. The last part of Eq. 30 is the derivative of the solute composition field along the radial direction estimated at the Ω^{pm} interface of radial position $r = R + \delta\ Y_{(l)}^{(m)}$. Eq. (30) is developed considering the r value at the interface and restricting development in derivative expression to the terms of first order associated to the main radius, R, and second order associated to instability, $\delta\ Y_{(l)}^{(m)}$. In addition, the velocity in the radial direction is the time derivative of the current radius $R + \delta\ Y_{(l)}^{(m)}$. The balance equation at the interface consequently develops as:

$$\left(X_{i,\kappa}^{mp} - X_{i,\kappa}^{pm}\right)\left(\dot{R} + \dot{\delta}\ Y_{(l)}^{(m)}\right) = -\frac{2\ \lambda^2}{R}\times \sum_{j=1}^{N} U_{ij}\left[\zeta_{j,(0)} F'_{(0)}\left(u_j\right) Y_{(0)}^{(0)} + \delta Y_{(l)}^{(m)}\left(\zeta_{j,(l)}\ F'_{(l)}\left(u_j\right) + \frac{2\ u_j}{R}\zeta_{j,(0)} F''_{(0)}\left(u_j\right) Y_{(0)}^{(0)} + \frac{1}{R}\ \zeta_{j,(0)}\ F'_{(0)}\left(u_j\right)\ Y_{(0)}^{(0)}\right)\right] \tag{31}$$

We separate the terms associated to the development of the main radius, $\dot{R}$, from those associated to the development of instabilities, $\dot{\delta}\ Y_{(l)}^{(m)}$. After some calculations and simplifications we obtain the relations for any solute specie i:

$$\left(X_{i,\kappa}^{mp} - X_{i,\kappa}^{pm}\right)\dot{R} = -\frac{2\ \lambda^2}{R}\sum_{j=1}^{N} U_{ij}\ \zeta_{j,(0)}\ F'_{(0)}\left(u_j\right) Y_{(0)}^{(0)} \tag{32}$$

$$\left(X_{i,\kappa}^{mp} - X_{i,\kappa}^{pm}\right)\dot{\delta} = \delta\left(X_{i,\kappa}^{mp} - X_{i,\kappa}^{pm}\right)\frac{\dot{R}}{R} - \frac{2\lambda^2\delta}{R}\sum_{j=1}^{N} U_{ij}\left(\frac{2\ u_j}{R}\zeta_{j,(0)} F''_{(0)}\left(u_j\right) Y_{(0)}^{(0)} + \zeta_{j,(l)} F'_{(l)}\left(u_j\right)\right) \tag{33}$$

where Eq. (32) is the interfacial solute balance for the sphere of radius R that has been injected in Eq. (33). Equations (28), (29), (32) and (33) compose a system of $2(N+1)$ linear relations with the $2(N+1)$ associated unknown $\dot{\delta}$, $\dot{R}$, $\zeta_{j,(0)}$ and $\zeta_{j,(l)}$. Consequently, the system may be solved in order to determine the temporal variations of the radius and the perturbation. It is worth noticing that $\zeta_{j,(0)}$ and $\zeta_{j,(l)}$ do not have the same unit and directly account for the effect of curvature as they are expressed as function of interfacial compositions $X_{i,\kappa}^{mp}$ and $X_{i,\kappa}^{pm}$. As shown in the appendix A, the system may be rewritten as Eq. (A.8):

$$\sum_{i=1}^{N} m_i \sum_{j=1}^{N} U_{ij}\left(-2\left(\frac{\dot{\delta}}{\delta}\frac{R}{\dot{R}} - 1\right)\frac{F_{(l)}\left(u_j\right)}{F'_{(l)}\left(u_j\right)} + 4\ u_j\left(\frac{F''_{(0)}\left(u_j\right)}{F'_{(0)}\left(u_j\right)}\frac{F_{(l)}\left(u_j\right)}{F'_{(l)}\left(u_j\right)} - 1\right)\right)\sum_{k=1}^{N} U_{jk}^{-1}\left(X_{k,\kappa}^{mp} - X_{k,\kappa}^{pm}\right) = \frac{(l+2)(l-1)}{\frac{R}{R^*} - 1}\ {}^{\mathbf{t}}\mathbf{m}\cdot\mathbf{U}\cdot\boldsymbol{\mathcal{F}}_{\mathbf{(0)}}\cdot\mathbf{U}^{-\mathbf{1}}\cdot\boldsymbol{\Delta}\mathbf{X}^{\mathbf{mp}} \tag{34}$$

where $\mathbf{m}$ is the vector of components m_i with $i \in \{1, N\}$ and $\boldsymbol{\mathcal{F}}_{\mathbf{(0)}}$ is a diagonal matrix of components introduced in Appendix A:

$$\mathcal{F}_{(0)_{ii}} = \frac{F_{(0)}\left(u_i\right)}{F'_{(0)}\left(u_i\right)} \tag{35}$$

2.3. Instability criteria

Thanks to the above mathematical developments we are now able to express the two criteria associated with the development of instabilities for a growing sphere [5]:

$$\begin{cases} \dot{\delta} > 0 \Rightarrow R > R_a \\ \dfrac{\dot{\delta}/\delta}{\dot{R}/R} > 1 \Rightarrow R > R_r \end{cases} \tag{36}$$

The first criterion is named *absolute stability*. It is associated to the development of perturbations not accounting for the growth of the particle. The threshold radius is then denoted R_a. The second criterion compares the development of the perturbations with the growth of the particle [9]. It is named *relative stability* and is related to the threshold radius R_r. The absolute stability leads to the following relation considering Eq. (34):

$$\frac{R_a}{R^*} = 1 + (l+2)(l-1)\frac{{}^{\mathbf{t}}\mathbf{m}\cdot\mathbf{U}\cdot\boldsymbol{\mathcal{F}}_{\mathbf{(0)}}\cdot\mathbf{U}^{-\mathbf{1}}\cdot\boldsymbol{\Delta}\mathbf{X}^{mp}}{{}^{\mathbf{t}}\mathbf{m}\cdot\mathbf{U}\cdot\boldsymbol{\mathcal{F}}_{\boldsymbol{\mathcal{H}}_{(l)}}\cdot\mathbf{U}^{-\mathbf{1}}\cdot\boldsymbol{\Delta}\mathbf{X}^{mp}} \tag{37}$$

where the $\boldsymbol{\mathcal{F}}_{\boldsymbol{\mathcal{H}}_{(l)}}$ is the diagonal matrix with non-zero components associated to u_i values:

$$\mathcal{F}_{\mathcal{H}_{(l)_{ii}}} = \frac{\mathcal{F}_{(0)_{ii}}}{\mathcal{H}_{(l)}(u_i)} \tag{38}$$

and the $\mathcal{H}_{(l)}$ function is defined by:

$$\mathcal{H}_{(l)}(x) = \frac{F_{(0)}(x)\ F'_{(l)}(x)}{2\ F_{(l)}(x)\ F'_{(0)}(x) + 4\ x\left[F''_{(0)}(x)\ F_{(l)}(x) - F'_{(l)}(x)\ F'_{(0)}(x)\right]} \tag{39}$$

Similarly, the relative stability criterion can be developed also considering Eq. (34):

$$\frac{R_r}{R^*} = 1+(l+2)(l-1)\frac{{}^{\mathbf{t}}\mathbf{m}\cdot\mathbf{U}\cdot\boldsymbol{\mathcal{F}}_{\mathbf{(0)}}\cdot\mathbf{U}^{-1}\cdot\boldsymbol{\Delta}\mathbf{X}^{mp}}{{}^{\mathbf{t}}\mathbf{m}\cdot\mathbf{U}\cdot\boldsymbol{\mathcal{F}}_{\boldsymbol{\mathcal{J}}_{(l)}}\cdot\mathbf{U}^{-1}\cdot\boldsymbol{\Delta}\mathbf{X}^{mp}} \tag{40}$$

where $\boldsymbol{\mathcal{F}}_{\boldsymbol{\mathcal{J}}_{(l)}}$ is the diagonal matrix with non-zero components associated to u_i values:

$$\mathcal{F}_{\mathcal{J}_{(l)}\,ii} = \frac{\mathcal{F}_{(0)\,ii}}{\mathcal{J}_{(l)}(u_i)} \tag{41}$$

and the $\mathcal{J}_{(l)}$ function is defined by:

$$\mathcal{J}_{(l)}(x) = \frac{F_{(0)}(x)F'_{(l)}(x)}{4\ x\left(F''_{(0)}(x)F_{(l)}(x) - F'_{(0)}(x)F'_{(l)}(x)\right)} \tag{42}$$

Comparing Eqs (37) and (40), one can notice that expressions for R_a and R_r only differ by functions $\boldsymbol{\mathcal{F}}_{\boldsymbol{\mathcal{H}}_{(l)}}$ and $\boldsymbol{\mathcal{F}}_{\boldsymbol{\mathcal{J}}_{(l)}}$ as given by Eqs (38) and (41), themselves only distinguished by functions $\mathcal{H}_{(l)}$ (Eq. 39) and $\mathcal{J}_{(l)}$ (Eq. 42). It is therefore of prime importance to study these functions prior to consider applications. This is done in the next section.

3. Validation

Expressions for R_a and R_r respectively given by Eqs (37) and (40) are first compared with previous criteria given in the literature [5, 11, 6, 7].

3.1. Steady regime approximations

The present unsteady solutions must retrieve the steady state regime studied for a binary alloy by Mullins and Sekerka [5] and for a ternary alloy by Colin and Vorhees [11] when all dimensionless growth parameters for solute specie i tend toward zero, $u_i \to 0$. In such conditions, the temporal derivatives of the composition field can be neglected so that Eq. (1) resumes to the Laplace equation. Note that this configuration corresponds to low values of the growth parameter λ, i.e. low growth rates. As demonstrated in appendix B, the limit associated to function $\mathcal{H}_{(l)}$ (Eq. (39)) is given by:

$$\lim_{x\to 0_+}\mathcal{H}_{(l)}(x) = \frac{1}{2}\frac{l+1}{l-1} \qquad \forall\ l \geq 2 \tag{43}$$

This limit is indeed retrieved in Fig. 2(a) for low x values. It can be used when expressing the $H_{(l)}(u_i)$ value (Eq. (37)) in the diagonal component of the $\boldsymbol{\mathcal{F}}_{\boldsymbol{\mathcal{H}}_{(l)}}$ matrix (Eq. (38)) for any u_i value. Also considering that:

$$\mathcal{F}_{(0)} \underset{0_+}{\sim} -2\ x \tag{44}$$

the numerator and denominator of the ratio in Eq. (37) for low u_i values consequently resume to the following relations:

$$\begin{aligned} &{}^{\mathbf{t}}\mathbf{m}\cdot\mathbf{U}\cdot\boldsymbol{\mathcal{F}}_{\mathbf{(0)}}\cdot\mathbf{U}^{-1}\cdot\boldsymbol{\Delta}\mathbf{X}^{mp} \\ &\sim -2\ {}^{\mathbf{t}}\mathbf{m}\cdot\mathbf{U}\cdot\boldsymbol{u}\cdot\mathbf{U}^{-1}\cdot\boldsymbol{\Delta}\mathbf{X}^{mp} \end{aligned} \tag{45}$$

$$\begin{aligned} &{}^{\mathbf{t}}\mathbf{m}\cdot\mathbf{U}\cdot\boldsymbol{\mathcal{F}}_{\boldsymbol{\mathcal{H}}_{(l)}}\cdot\mathbf{U}^{-1}\cdot\boldsymbol{\Delta}\mathbf{X}^{mp} \\ &\sim -4\frac{l-1}{l+1}\ {}^{\mathbf{t}}\mathbf{m}\cdot\mathbf{U}\cdot\boldsymbol{u}\cdot\mathbf{U}^{-1}\cdot\boldsymbol{\Delta}\mathbf{X}^{mp} \end{aligned} \tag{46}$$

where the $\boldsymbol{u}$ matrix stands for the diagonal matrix with u_i components. The following limit for the absolute stability criterion is then obtained:

$$\lim_{\lambda\to 0_+}\frac{R_a}{R^*} = 1+\frac{1}{2}(l+1)(l+2) \qquad \forall\ N \tag{47}$$

This limit is nothing but the ratio provided by Mullins and Sekerka [5] associated to the absolute stability for any given l value. The lowest possible value for the degree of the spherical harmonics is $l = 2$. It corresponds to the lowest ratio $R_a/R^* = 7$ associated to a perturbation at the onset of the instability. These values depend neither from the number of components, N, nor from the physical properties of the alloy, as previously found for binary alloys [5] and ternary alloys [11]. Illustration of these limits at low velocity are given in Fig. 3(a).

Similarly, the following limit is obtained for function $\mathcal{J}_{(l)}$ (Eq. 42) as derived in Appendix C and illustrated in Fig. 2(b):

$$\lim_{x\to 0_+}\mathcal{J}_{(l)}(x) = \frac{1}{2}\frac{l+1}{l-2} \qquad \forall\ l \geq 3 \tag{48}$$

Using this relation, we develop the denominator of Eq. (40) at low u_i values:

$$\begin{aligned} &{}^{\mathbf{t}}\mathbf{m}\cdot\mathbf{U}\cdot\boldsymbol{\mathcal{F}}_{\boldsymbol{\mathcal{J}}_{(l)}}\cdot\mathbf{U}^{-1}\cdot\boldsymbol{\Delta}\mathbf{X}^{mp} \\ &\sim -4\frac{l-2}{l+1}\ {}^{\mathbf{t}}\mathbf{m}\cdot\mathbf{U}\cdot\boldsymbol{u}\cdot\mathbf{U}^{-1}\cdot\boldsymbol{\Delta}\mathbf{X}^{mp} \end{aligned} \tag{49}$$

Injecting the limits given by Eqs (45) and (49) in Eq. (40) leads to the following expression for the relative stability criterion:

$$\lim_{\lambda\to 0_+}\frac{R_r}{R^*} = \frac{l(l+1)^2-6}{2(l-2)} \qquad \forall\ N \tag{50}$$

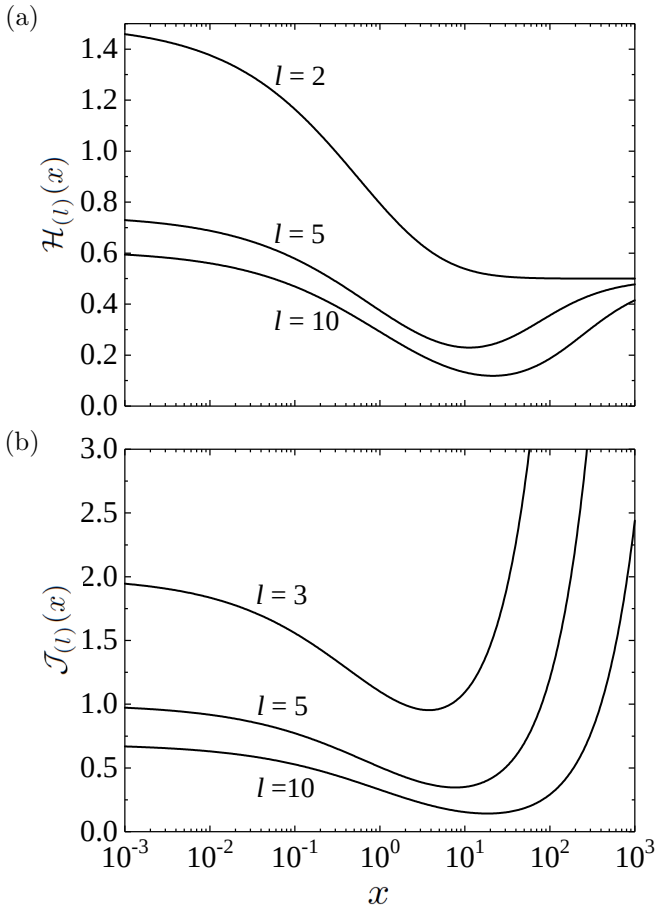

Figure 2: Evolution of the functions (a) $\mathcal{H}_{(l)}(x)$ (Eq. 39) and (b) $\mathcal{J}_{(l)}(x)$ (Eq. 42) for different values of the degree, l, of the spherical harmonic function.

The latter expression also corresponds to the limit read on the curves shown in Fig. 3(a) for low x values. As before, we thus validate the present development by retrieving the results by Mullins and Sekerka [5] for the relative stability regime for any l value. Similar expression was also provided by Colin and Voorhees [11] for ternary alloys. As the ratio is meaningless for $l = 2$, the lowest ratio is obtained for $l = 3$ leading to $R_r/R^* = 21$ for any number of components, thus defining the threshold radius for the relative stability regime.

We can also develop the mathematical expressions of the threshold radii associated to the absolute and relative stability regimes for large growth velocity, i.e. when $\lambda \to +\infty$. Indeed, using the limits for functions $\mathcal{F}_{\mathcal{H}_{(l)}}(x)$ and $\mathcal{F}_{\mathcal{J}_{(l)}}(x)$ at large x value given in Appendices B and C by Eqs (B.9) and (C.4), we demonstrate that:

$$\lim_{\lambda\to+\infty} \frac{R_a}{R^*} = 1 + \frac{1}{2}(l-1)(l+2) \qquad \forall\ N \tag{51}$$

$$\lim_{\lambda\to+\infty} \frac{R_r}{R^*} = +\infty \qquad \forall\ N \tag{52}$$

Again, these limits are illustrated in Fig. 3 for both criteria at large growth velocity. Regarding the first criterion, R_a/R^*, this may lead to consider a limit value of 3 as associated to the lowest acceptable l value of 2.

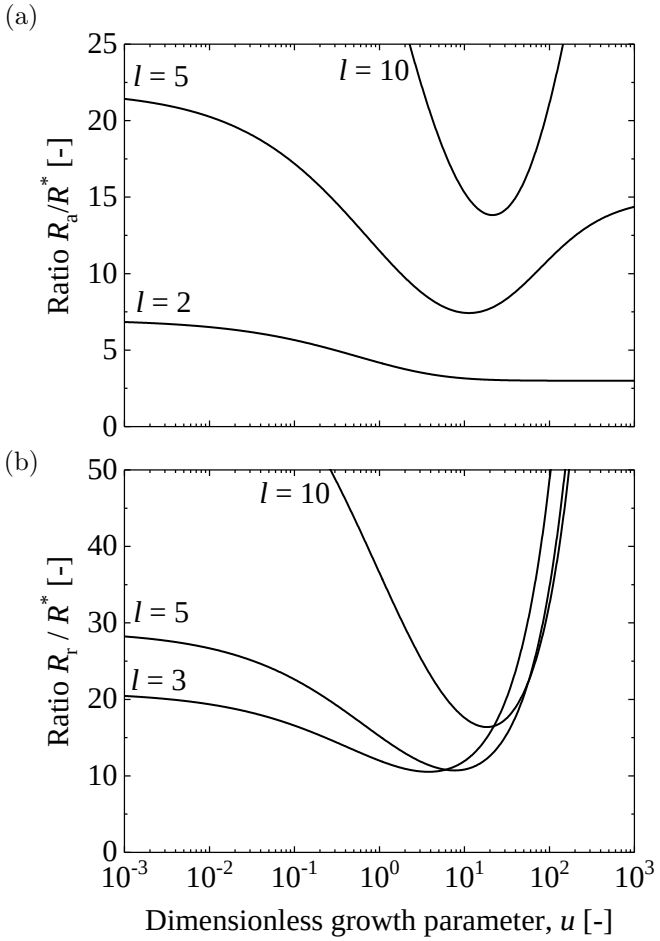

Figure 3: Evolution of the threshold radius defining the growth stability of a spherical particle considering both (a) the absolute stability criterion, R_a, and (b) the relative stability criterion, R_r, as a function of the dimensionless growth parameter u for a binary alloy. Curves are normalized by the critical nucleation radius, R^*, and are drawn for several values of the degree of the spherical harmonics, l.

3.2. Unsteady regime approximations

The general mathematical expressions for the stability criteria, Eqs (37) and (40), are valid under non steady growth regimes when the temporal derivative of the composition field is maintained as part of the solute conservation equation (Eq. (1)). These results are hereafter considered under the restriction of a binary alloy. In such conditions, simplifications arise for the expression associated to R_a and R_r:

$$\frac{R_a}{R^*} = 1 + (l+2)(l-1)\mathcal{H}_{(l)}(u) \tag{53}$$

$$\frac{R_r}{R^*} = 1 + (l+2)(l-1)\mathcal{J}_{(l)}(u) \tag{54}$$

where u is simply equal to λ^2/D^m, D^m being the diffusion coefficient in the matrix phase associated to the solute specie of the binary alloy. Again, these solutions are independent from the thermodynamic properties of the alloy for any given growth parameter λ. Fig. 3 shows the continuous evolution of the critical radii for both absolute and relative stability criteria and several l values. Although few developments are reported in literature to investigate the stability domains in unsteady growth regime, the original approach by Wey et al. [6, 7] may be considered. Considering our own notations of the critical radius and further neglecting the kinetics undercooling, they found:

$$\frac{R_a}{R^*} = 1 + \frac{1}{u\ G(u)} \frac{(u - 2\ l - 2)(l + 2)(l - 1) - 2\ u}{u - 2\ l + 2} \quad (55)$$

$$\frac{R_r}{R^*} = 1 + \frac{1}{u\ G(u)} \frac{(u - 2\ l - 2)(l + 2)(l - 1) - 2\ u}{u\ \ - 2\ l + \ 4} \quad (56)$$

Associated evolution are reported using black lines in Fig. 4 for a set of l values similar to the one applied in Fig. 3. Results of Fig. 3 corresponding to the present solutions are added in dashed grey color so as to ease the comparison with the results by Wey et al. [6, 7]. For low growth velocity, when $u \to 0_+$, similar tendencies are observed and curves are superimposed until $u \simeq 0.1$. At higher velocity, differences clearly appear. The expressions proposed by Wey et al. show a systematic dramatic increase of the critical radii for all l values. This is explained by the denominator of Eqs. (55) and (56) showing divergence of the results when $u = 2(l - 1)$ for R_a and $u = 2(l - 2)$ for R_r. The present work does not show such abrupt variations for any l value.

Results also provide access to the stability and instability domains for the growth of a spherical shape particle at a given velocity. This is done by considering the envelope of the curves drawn in Fig. 3 and 4 for R_a/R^* and R_r/R^* ratios leading to stable developments. Such domains are draw in Fig. 5(a) and (c) using the present expressions, Eqs (37) and (40), and in Fig. 5(b) and (d) using the mathematical expressions by Wey et al. [6, 7], Eqs (55) and (56).

Similar stability domains are drawn at low growth velocity ($u \to 0_+$) for both criteria. On the contrary differences are observed at higher growth velocity. As shown in Fig. 5(a), the absolute stability domain is limited by the curve $l = 2$ in Fig. 3(a). Consequently, this domain reduces for higher velocity and R_a tends to 3 R^* (Eq. (51) with $l = 2$). On the contrary, the stability domain is surrounded by two instability domains for the same criterion according to Wey et al. (Fig. 5(b)). For the relative stability criterion, similar tendency is found when comparing Fig. 5(c) and 5(d). Thus, with the solution by Wey et al. [6, 7], the unstable domain is discontinuous. Such results

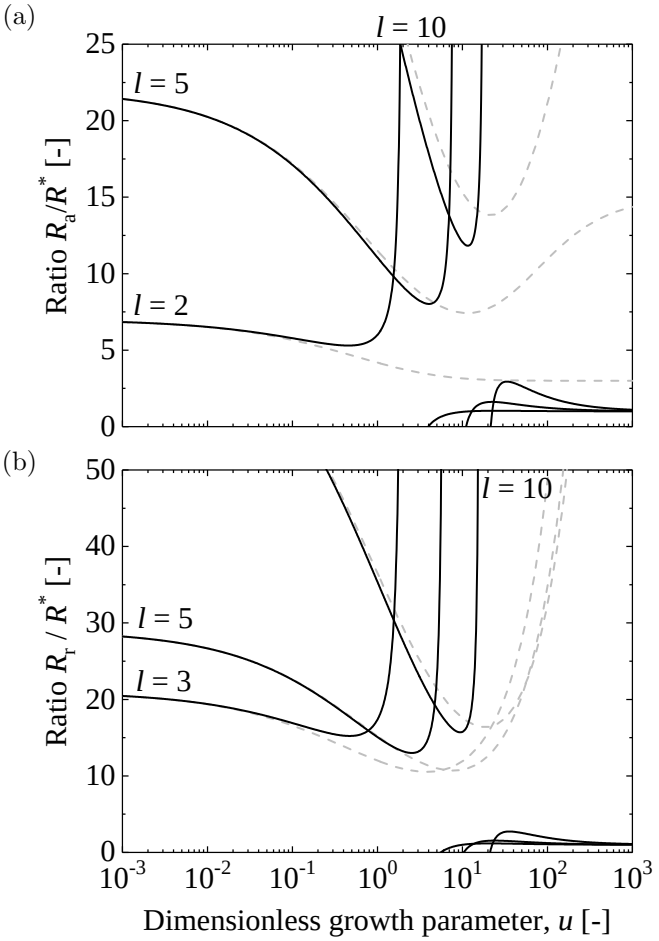

Figure 4: Evolution of the threshold radius defining the growth stability of a spherical particle considering both (a) the absolute stability criterion, R_a, and (b) the relative stability criterion, R_r, as a function of the dimensionless growth parameter u for a binary alloy. Curves are normalized by the critical nucleation radius, R^*, and are drawn for several values of the degree of the spherical harmonic function, l. Black curves refer to the solutions proposed by Wey et al. ([6, 7]), Eqs (55) and (56), and dashed grey curves to the present results, Eqs (37) and (40).

is not well explained by the authors, nor is it believed to be reasonable.

Finally, the present analysis can provide information on the wave number associated to the development of instabilities. Indeed, the threshold ratio R_r/R^* associated to the occurrence of instabilities at the surface of a spherical particles is linked to a given degree l of the spherical harmonic function. The evolution of this value, corresponding to the wave number of perturbations that may develop on the interface can thus be estimated. Fig. 6 shows the evolution of the l value as a function of the dimensionless growth parameter. An exponential evolution is observed as the number of oscillations on a spherical particle rapidly increases for high velocity, also corresponding to higher value of the supersaturation. In practice, this means that a higher degree of the harmonic function is expected for

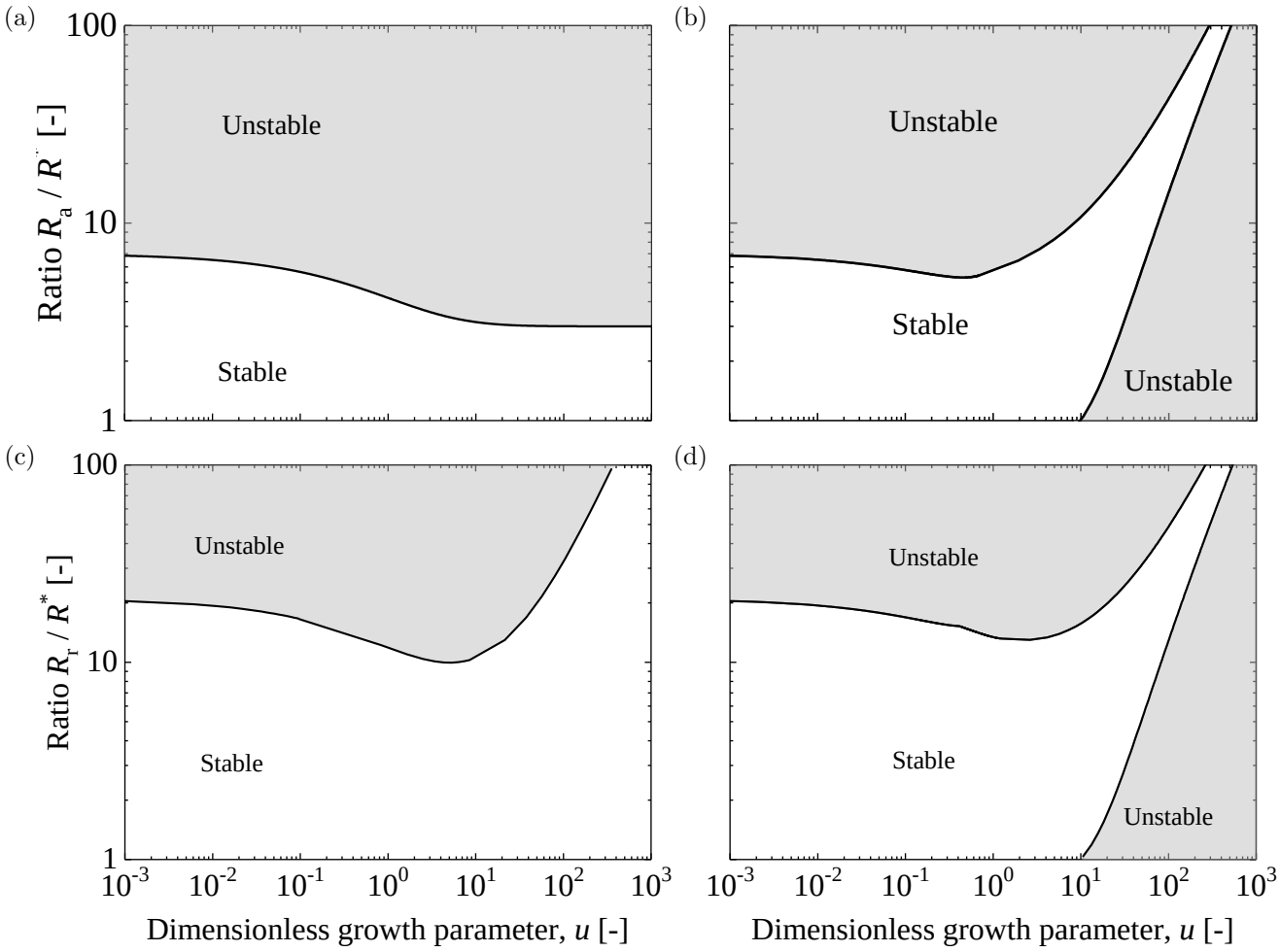

Figure 5: Stable and unstable domains associated to the development of perturbations for both the (a,b) absolute and (c,d) relative criteria using (a,c) the present results and (b,d) the work by Wey et al. [6, 7].

instability at high supersaturation.

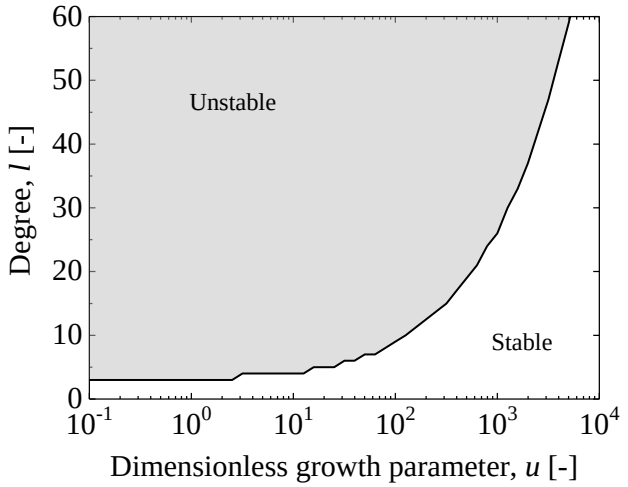

Figure 6: Degree, l, of the spherical harmonic function, $Y_{(l)}^{(m)}$, associated to the development of instabilities with the relative stability criterion as a function of the dimensionless growth parameter.

Property	Variable	Value	Unit
Nominal composition			
Si	$X_{Si,0}$	7	(wt.%)
Mg	$X_{Mg,0}$	1	(wt.%)
Liquidus slope			
Si	m_{Si}	-6.67	$(\mathrm{K}\cdot\mathrm{wt.\%}^{-1})$
Mg	m_{Mg}	-4.24	$(\mathrm{K}\cdot\mathrm{wt.\%}^{-1})$
Partition coefficient			
Si	k_{Si}	0.107	$(\mathrm{wt.\%}\cdot\mathrm{wt.\%}^{-1})$
Mg	k_{Mg}	0.221	$(\mathrm{wt.\%}\cdot\mathrm{wt.\%}^{-1})$
Melting temperature	T_M	936.38	(K)
Liquidus temperature	T_L	885.45	(K)
Density	ρ	2552	$(\mathrm{kg}\cdot\mathrm{m}^{-3})$

Table 1: Properties of the linear ternary phase diagram for the Al-7wt.%Si-1wt.%Mg alloy [15] defining F_κ^{mp} through Eq. (25) and F_κ^{pm} by the partition coefficients of the solute species with $X_{i,\kappa}^{pm} = k_i X_{i,\kappa}^{mp}$

.

4. Application

An application is now proposed in order to highlight the effect of various diffusion matrices on the evolution of the absolute and relative stability criteria. The ternary system Al-7wt.%Si-1wt.%Mg is investigated under solidification. That is, the matrix m is the liquid phase, denoted l, and the particle p is an aluminum rich solid phase of face-centered cubic crystallographic structure, denoted s. The physical properties of the alloy previously defined in [1] are reproduced in Table 1. The full diffusion matrix associated to the solute species Si and Mg in the liquid phase, $\mathbf{D}^l$, is given in Table 2 together with its associated eigenvalues, $\mathbf{B}^l$, and eigenvectors $\mathbf{U}^l$. Three other diffusion matrices are also given in Table 2. They are chosen so as to illustrate the effect of the cross diffusion terms. Matrices $\mathbf{D}_{inf}^l$ and $\mathbf{D}_{sup}^l$ are respectively defined with $D_{SiMg}^l = 0$ and $D_{MgSi}^l = 0$ while $\mathbf{D}_{dia}^l$ is simply a diagonal approximation of the full diffusion matrix $\mathbf{D}^l$ where the off diagonal terms have been set to zero.

Fig. 7 shows the evolution of the growth parameter, λ, as a function of the temperature T computed from resolution of Eq. 6 also considering thermodynamic equilibrium between solid and liquid phases (Tab. 1). Evolution of the growth parameter are shown to depend from the choice of the diffusion matrix. Some differences are consequently observed between curves mainly for low temperature regime or high growth rate. It is noticeable that, unlike the previous session, representation with the dimensionless growth parameter u_{Si} and u_{Mg} requires three dimensional representations. This is why the choice of the common growth parameter λ is made, also corresponding to a unique temperature defined by the corresponding set of $\mathbf{X}^{mp}$ composition for a given radius according to Eq. (3).

The normalized absolute and relative stability ratios are presented as a function of both the growth parameter and the temperature for the same four diffusion matrices. Regarding the absolute stability ratio show in Fig. 8(a), the same threshold values of 7 at low growth rate and 3 at high growth rate are retrieved for all diffusion matrices. These limits are the ones respectively estimated in Eq. (47) and Eq. (51) for $l = 2$. As previously shown in Fig. 7, the low growth rate limit in Fig. 8(b) is found for high temperature (close to the liquidus temperature) when $\lambda \simeq 0$ while the high growth rate limit corresponds to low temperature. Also to be noticed in Fig. 8(a) and (b) is the separate evolution of the curve for the full matrix $\mathbf{D}^l$ compared to other matrices, probably due to the difference in its eigenvalues (Tab. 2).

Calculations for the normalized relative stability ratio are displayed in Fig. 8(c) and (d). Again, the expected limits at low/high growth velocity are found, respectively 21 at the liquidus temperature and infinity at very low temperature. These values are in accordance with previous estimations done in Eq. (50) for $l = 3$ and in Eq. (52). Evolution associated to $\mathbf{D}^l$ matrix is still different compared to other three matrices. However, a more complex behavior is observed at intermediate growth parameter and temperature. A minimum value is predicted for the relative stability ratio at temperature $T \simeq 825 \sim 850$ K or $\lambda \simeq 80 \sim 120$ μm.s$^{-1/2}$ when the ratio is close to 10. This corresponds to an increase of the instability domain that may be prone to the development of perturbations on the solid/liquid interface and changes in final grain morphology.

Diffusion matrix $[10^{-9}\ \mathrm{m}^2 \cdot \mathrm{s}^{-1}]$								
	$\mathbf{D}^l$		$\mathbf{D}^l_{inf}$		$\mathbf{D}^l_{sup}$		$\mathbf{D}^l_{dia}$	
Si	2.277	3	2.277	0	2.277	3	2.277	0
Mg	2	5.914	2	5.914	0	5.914	0	5.914
	Si	Mg						
Eigenvalues $[10^{-9}\ \mathrm{m}^2 \cdot \mathrm{s}^{-1}]$								
	$\mathbf{B}^l$		$\mathbf{B}^l_{inf}$		$\mathbf{B}^l_{sup}$		$\mathbf{B}^l_{dia}$	
	1.045	7.146	2.277	5.914	2.277	5.914	2.277	5.914
Eigenvectors								
	$\mathbf{U}^l$		$\mathbf{U}^l_{inf}$		$\mathbf{U}^l_{sup}$		$\mathbf{U}^l_{dia}$	
Si	0.925	0.525	0.876	0	1	0.636	1	0
Mg	−0.380	0.851	−0.482	1	0	0.771	0	1
	Si	Mg						

Table 2: Diffusion matrices, $\mathbf{D}$, in the liquid phase. Eigenvalues, $\mathbf{B}$, and associated eigenvectors, $\mathbf{U}$, in liquid diffusion matrices are also provided for the first (Si) and the second (Mg) component. [15, 16]

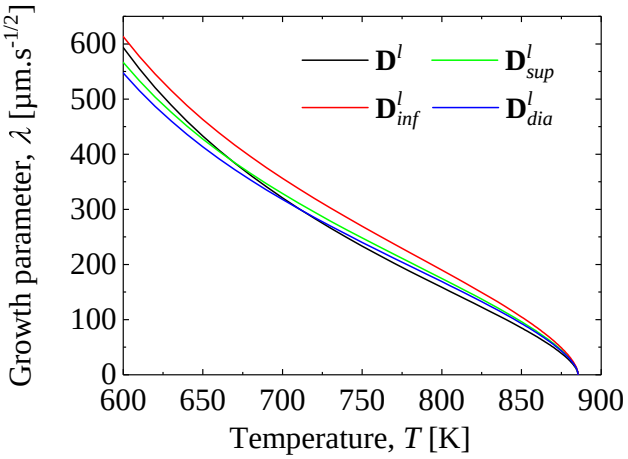

Figure 7: Evolution of the growth parameter, λ, depending from the temperature, T, for the ternary alloy Al-7wt.%Si-1wt.%Mg. Four diffusion matrices are investigated.

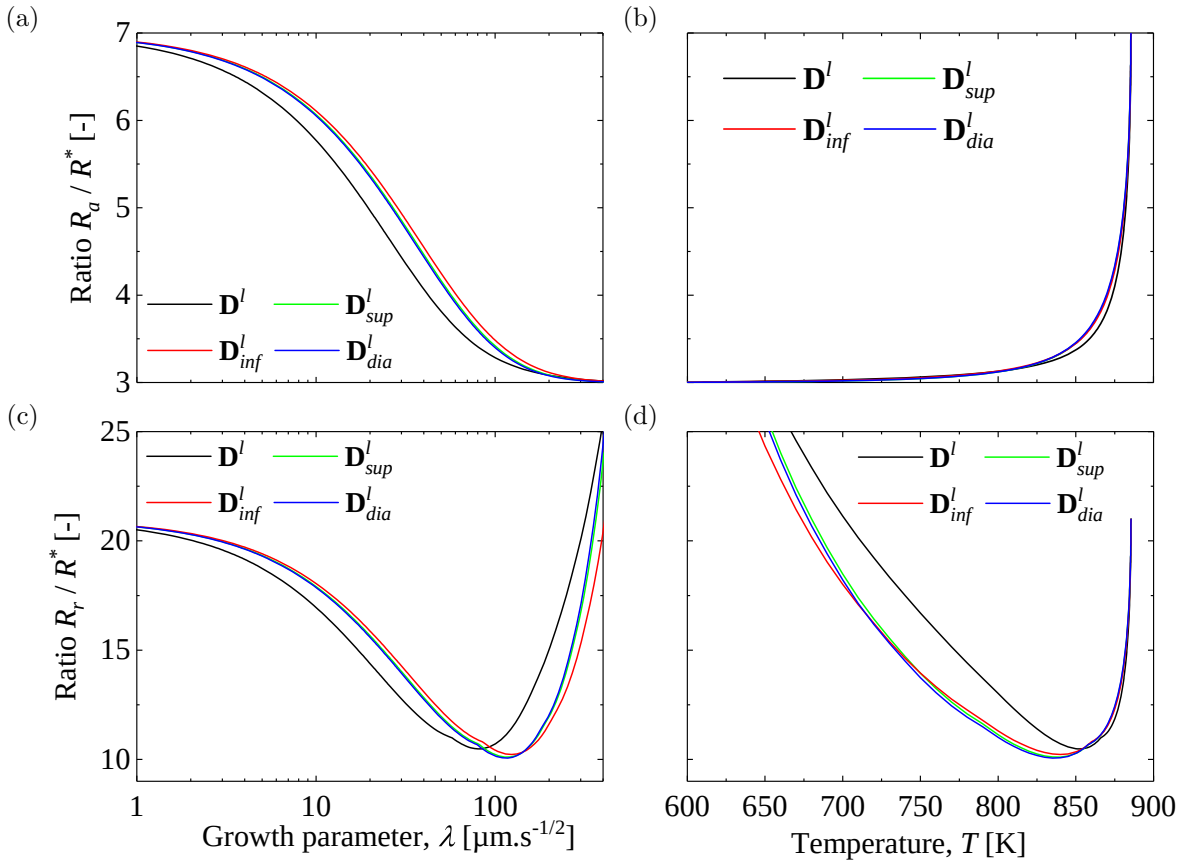

Figure 8: Evolution of (a,b) absolute and (c,d) relative stability ratios for the threshold stability value of the growth radius of a sphere in a ternary Al-7wt.%Si-1wt.%Mg alloy as a function of (a,c) the growth parameter, λ, and (b,d) the temperature, T . Four diffusion matrices are investigated, as reported in Table 2.

5. Conclusion

The stability analysis of a growing sphere is developed for a multicomponent alloy. The sphere represents a particle embedded in a matrix assumed of infinite size so its far-field composition is maintained constant. Growth proceeds due to mass exchange at the interface between the particle and the matrix and diffusion in the matrix phase. The analysis differs from previous work by the following main differences:

i– a full diffusion matrix is considered so cross diffusion terms for the diffusion fluxes are not neglected,

ii– the conservation of the solute species is written in full, i.e. not with the usual approximation that consists of neglecting the time derivative and thus reducing the problem to the solution of the Laplace equation [5, 11].

As a result, the criteria for stability are not reduced to low velocity values as this was the case in previous work [5, 11]. So the stability of the growing sphere can be considered for nucleation and growth at high supersaturation or high growth rate. The results clearly show that the threshold values for the destabilization of the interface of a growing sphere strongly depends on the supersaturation. The degree of the spherical harmonic at which stability is not maintained is also found to increase with the supersaturation. Finally, the role of the approximation consisting of using a diagonal diffusion matrix is illustrated for the particular situation of a solid particle formed in a liquid phase in the ternary system Al-7wt.%Si-1wt.%Mg.

Further work on the stability analysis for industrial alloys could benefit from the present developments and could be compared with numerical simulations [12]. Extension of the present methodology to the stability analysis of planar front could also be developed, thus extending the work by Hunziker [17].

Nomenclature

Latin symbols

$\mathbf{B}$	diagonalized diffusion matrix	$\mathrm{m}^2 \cdot \mathrm{s}^{-1}$
$B_\bullet$	eigenvalue of the diffusion matrix	$\mathrm{m}^2 \cdot \mathrm{s}^{-1}$
$\mathbf{D}$	diffusion matrix	$\mathrm{m}^2 \cdot \mathrm{s}^{-1}$
k	segregation coefficient	-
m	liquidus slope	$\mathrm{K} \cdot \mathrm{at.}\%^{-1}$
N	number of added elements	-
r	radial coordinate	m
R	growth radius - no perturbation	m
t	time	s
T	temperature	K
u	dimensionless growth parameter	-
$\mathbf{U}_\bullet$	eigenvector of the diffusion matrix	-
$\mathbf{U}$	transfer matrix	-
v	growth velocity	$\mathrm{m} \cdot \mathrm{s}^{-1}$
V_m	molar volume	$\mathrm{m}^3 \cdot \mathrm{mol}^{-1}$
X	molar composition	at.%
$\widetilde{X}$	intermediate variable	at.%
Y	spherical harmonic function	-

Greek symbols

δ	amplitude of perturbation	m
$\mathbf{\Delta X}_0^m$	difference in matrix composition between interface and large distance	at.%
$\mathbf{\Delta X}_0^{mp}$	difference in composition between matrix and particle at the interface	at.%
κ	curvature	m^{-1}
Ω	domain	-
φ, θ	coordinates angles	rad
λ	growth parameter	$\mathrm{m} \cdot \mathrm{s}^{-1/2}$
Γ	Gibbs-Thomson coefficient	$\mathrm{K} \cdot \mathrm{m}$
Λ	matrix defining the interfacial composition difference	-
$\zeta_{.,(0)}$	unknown factor associated to fundamental solution - unperturbed geometry	at.%

$\zeta_{.,(l)}$ unknown factor associated to harmonic solutions - perturbed geometry at.% $\cdot$ m^{-1}

Superscripts

α phase

l liquid phase

(m) order of spherical harmonic functions

m matrix phase

p particle phase

pm particle\matrix interface

s solid phase

sl solid liquid interface

$*$ nucleation

Subscripts

a absolute stability

dia, sup, inf matrix type

i, j, k component

(l) degree of spherical harmonic functions

r relative stability

∞ variable at large distance

Mathematical notations

erfc(.) complementary error function

P(.) associated Legendre polynomial

$\Gamma(.)$ gamma function

$\Gamma(.,.)$ incomplete gamma function

$\mathcal{H}_{(l)}(.)$ function associated to absolute stability

$\mathcal{J}_{(l)}(.)$ function associated to relative stability

$\nabla^2(.)$ Laplace operator

$\Lambda(.)$ angular part of Laplace operator

$U[.]$ Tricomi's function

$W_{\kappa,\mu}(.)$ Whittaker function

Appendix A

We first invert the linear system presented in Eq. (32) in order to obtain:

$$-2\,\frac{\lambda^2}{R}\,\zeta_{i,(0)}\,F'_{(0)}\left(u_i\right)Y_{(0)}(0)=\dot{R}\sum_{j=1}^{N}U_{ij}^{-1}\left(X_j^{mp}-X_j^{pm}\right) \tag{A.1}$$

This expression provides direct estimation of $\zeta_{i,(0)}$ coefficients which can be used in Eq. (28):

$$-\sum_{i=1}^{N}m_i\,\Delta X_i^l-\frac{R\,\dot{R}}{2\,\lambda^2}\sum_{i=1}^{N}m_i\,\sum_{j=1}^{N}U_{ij}\,\frac{F_{(0)}\left(u_j\right)}{F'_{(0)}\left(u_j\right)}\sum_{k=1}^{N}U_{jk}^{-1}\left(X_k^{mp}-X_k^{pm}\right. \tag{A.2}$$

This expression is simplified considering the critical radius equation Eq. (26), and matrices expression as:

$$\frac{R}{R^*}-1=\frac{R^2\,\dot{R}}{4\,\lambda^2\,\Gamma}\,{}^{\mathbf{t}}\mathbf{m}\cdot\mathbf{U}\cdot\boldsymbol{\mathcal{F}}_{\mathbf{(0)}}\cdot\mathbf{U}^{-\mathbf{1}}\cdot\boldsymbol{\Delta}\mathbf{X}^{\mathbf{mp}} \tag{A.3}$$

where $\mathbf{m}$ vector refers to the set of $m_{i|1\leq i\leq N}$ component and $\boldsymbol{\mathcal{F}}_{\mathbf{(0)}}$ is a diagonal matrix with single non zero component:

$$\mathcal{F}_{(0)_{ii}}=\frac{F_{(0)}\left(u_i\right)}{F'_{(0)}\left(u_i\right)} \tag{A.4}$$

Similarly, equation (33) may be used in order to provide estimation of $\zeta_{i,(l)}$ unknown variables for any specie i. We inverse this relation firstly in order to provide the following equality:

$$\left(\frac{\dot{\delta}}{\delta}-\frac{\dot{R}}{R}\right)\sum_{j=1}^{N}U_{ij}^{-1}\left(X_j^{mp}-X_j^{pm}\right)=-\frac{4\,u_i\,\lambda^2}{R^2}\zeta_{i,(0)}\,F''_{(0)}\left(u_i\right)Y_{(0)}(0) \tag{A.5}$$

Using Eq. (A.1), we have an expression of $\zeta_{i,(0)}$ which leads to the relation:

$$\left(\frac{\dot{\delta}}{\delta}-\frac{\dot{R}}{R}-\frac{2\,\dot{R}\,\lambda^2}{R\,B_i^l}\frac{F''_{(0)}\left(u_i\right)}{F'_{(0)}\left(u_i\right)}\right)\sum_{j=1}^{N}U_{ij}^{-1}\left(X_j^{mp}-X_j^{pm}\right)=-\frac{2\,\lambda^2}{R}\,\zeta_{i,(} \tag{A.6}$$

This latter relation provides estimation of $\zeta_{i,(l)}$ coefficients which is introduced in Eq. (29), also considering expression of $\zeta_{i,(0)}$ (Eq. A.2), leading to:

$$\sum_{i=1}^{N}m_i\sum_{j=1}^{N}U_{ij}\left(-\left(\frac{\dot{\delta}}{\delta}-\frac{\dot{R}}{R}\right)\frac{R}{2\,\lambda^2}\,\frac{F_{(l)}\left(u_j\right)}{F'_{(l)}\left(u_j\right)}+\frac{\dot{R}}{B_j^l}\left(\frac{F''_{(0)}\left(u_j\right)}{F'_{(0)}\left(u_j\right)}\frac{F_{(l)}\left(\right.\right.\right.$$
$$=\frac{\Gamma}{R^2}(l+2)(l-1) \tag{A.7}$$

We may also consider the relation between radius, time radius evolution and critical radius (Eq. A.3). This relation leads to simplifications in previous expression as:

$$\sum_{i=1}^{N}m_i\sum_{j=1}^{N}U_{ij}\left(-2\left(\frac{\dot{\delta}}{\delta}\frac{R}{\dot{R}}-1\right)\frac{F_{(l)}\left(u_j\right)}{F'_{(l)}\left(u_j\right)}+4u_j\left(\frac{F''_{(0)}\left(u_j\right)}{F'_{(0)}\left(u_j\right)}\frac{F_{(l)}\left(u_j\right)}{F'_{(l)}\left(u_j\right)}\right.\right.$$
$$\underline{\forall}\,i\,\frac{(l+2)(l-1)}{\frac{R}{R^*}-1}\,{}^{\mathbf{t}}\mathbf{m}\cdot\mathbf{U}\cdot\boldsymbol{\mathcal{F}}_{\mathbf{(0)}}\cdot\mathbf{U}^{-\mathbf{1}}\cdot\boldsymbol{\Delta}\mathbf{X}^{\mathbf{mp}} \tag{A.8}$$

Appendix B

After some mathematical development, the $\mathcal{H}_{(l)}$ function is expressed for any x value as:

$$\mathcal{H}_{(l)}(x) = \frac{1}{8}\sqrt{x}\, e^{x/4}\, \Gamma\left(-\frac{1}{2}, \frac{x}{4}\right) \frac{(3+l)\,(l-2)\, W_{-\frac{7}{4},\frac{1}{4}+\frac{l}{2}}\left(\frac{x}{4}\right) + (x+6)\, W_{-\frac{3}{4},\frac{1}{4}+\frac{l}{2}}\left(\frac{x}{4}\right)}{(3+l)\,(l-2)\, W_{-\frac{7}{4},\frac{1}{4}+\frac{l}{2}}\left(\frac{x}{4}\right) + 2(x+6)\, W_{-\frac{3}{4},\frac{1}{4}+\frac{l}{2}}\left(\frac{x}{4}\right)} \tag{B.1}$$

where Γ is the incomplete Gamma function and $W_{\kappa,\mu}$ is the Whittaker function of parameters κ and μ [13]. Fig (2 a) shows the evolution of the $\mathcal{H}_{(l)}$ function for various l values. We may have firstly to estimate the limit of function $\mathcal{H}_{(l)}(x)$ for low x values. The following approximation [13] stands for low values of z variable:

$$\Gamma\left(-\frac{1}{2}, z\right) \sim \frac{2}{\sqrt{z}} \quad \text{if} \quad z \to 0_+ \tag{B.2}$$

-

$$W_{\kappa,\mu}(z) \sim \frac{\Gamma(2\,\mu)}{\Gamma\left(\mu-\kappa+\frac{1}{2}\right)} \frac{1}{z^{\mu-1/2}} \quad \text{if} \quad z \to 0_+, \quad \forall\, \mu > 0 \tag{B.3}$$

where Γ is the gamma function. We may consequently estimate if $x \to 0_+$:

$$\begin{aligned} \Gamma\left(-\frac{1}{2}, \frac{x}{4}\right) &\sim \frac{4}{\sqrt{x}} \\ W_{-\frac{7}{4},\frac{1}{4}+\frac{l}{2}}\left(\frac{x}{4}\right) &\sim \frac{\Gamma(\frac{1}{2}+l)}{\Gamma\left(\frac{5}{2}+\frac{l}{2}\right)} \left(\frac{x}{4}\right)^{\frac{1}{4}-\frac{l}{2}} \\ W_{-\frac{3}{4},\frac{1}{4}+\frac{l}{2}}\left(\frac{x}{4}\right) &\sim \frac{\Gamma(\frac{1}{2}+l)}{\Gamma\left(\frac{3}{2}+\frac{l}{2}\right)} \left(\frac{x}{4}\right)^{\frac{1}{4}-\frac{l}{2}} \end{aligned} \tag{B.4}$$

The $\mathcal{H}_{(l)}$ function can be approximated at low x value using these relations. After some mathematical developments not detailed thereafter, we obtain the following limit:

$$\lim_{x\to 0_+} \mathcal{H}_{(l)}(x) = \frac{1}{2}\frac{l+1}{l-1} \qquad \forall\, l \geq 2 \tag{B.5}$$

Similarly, we have the following approximations at large z value:

$$\Gamma\left(-\frac{1}{2}, z\right) \sim \frac{e^{-z}}{z^{3/2}} \quad \text{if} \quad z \to +\infty \tag{B.6}$$

$$W_{\kappa,\mu}(z) \sim e^{-z/2} z^{\kappa} \quad \text{if} \quad z \to +\infty \tag{B.7}$$

We may consequently estimate if $x \to +\infty$:

$$\begin{aligned} \Gamma\left(-\frac{1}{2}, \frac{x}{4}\right) &\sim \frac{8\, e^{-x/4}}{x^{3/2}} \\ W_{-\frac{7}{4},\frac{1}{4}+\frac{l}{2}}\left(\frac{x}{4}\right) &\sim e^{-x/8} \left(\frac{x}{4}\right)^{-7/4} \\ W_{-\frac{3}{4},\frac{1}{4}+\frac{l}{2}}\left(\frac{x}{4}\right) &\sim e^{-x/8} \left(\frac{x}{4}\right)^{-3/4} \end{aligned} \tag{B.8}$$

After some mathematical developments based on Eq. (B.1), we obtain the following limit:

$$\lim_{x\to+\infty} \mathcal{H}_{(l)}(x) = \frac{1}{2} \tag{B.9}$$

This limit is highlighted on Fig. (2 a) for large λ value. Similarly, it also provides limit on the absolute stability criterion for large growth velocity.

Appendix C

After some developments, the $\mathcal{J}_{(l)}$ function can be expressed as:

$$\mathcal{J}_l(x) = \frac{1}{8}\sqrt{x}\, e^{x/4}\, \Gamma\left(-\frac{1}{2}, \frac{x}{4}\right) \left(1 + \frac{6+x}{l(l+1)-6} \frac{W_{-\frac{3}{4},\frac{1}{4}+\frac{l}{2}}\left(\frac{x}{4}\right)}{W_{-\frac{7}{4},\frac{1}{4}+\frac{l}{2}}\left(\frac{x}{4}\right)}\right) \tag{C.1}$$

Fig. (2 b) shows the evolution of the $\mathcal{J}_{(l)}$ function for various l values. When considering previous relations (Eq. B.4), the limit for $\mathcal{J}_{(l)}$ function at low x value can be estimated as:

$$\lim_{x\to 0_+} \mathcal{J}_{(l)}(x) = \frac{1}{2}\frac{l+1}{l-2} \qquad \forall\, l \geq 3 \tag{C.2}$$

Similarly, we use Eq. (B.8) to estimate the evolution of $\mathcal{J}_{(l)}(x)$ function at large x value, when $x \to +\infty$:

$$\mathcal{J}_{(l)}(x) \sim \frac{x}{4(l(l+1)-6)} \qquad \forall\, l \geq 3 \tag{C.3}$$

Consequently, we have the upper limit:

$$\lim_{x\to+\infty} \mathcal{J}_{(l)}(x) = +\infty \qquad \forall\, l \geq 3 \tag{C.4}$$

These limits are also highlighted on Fig. (2 b) as function $\mathcal{J}_{(l)}$ continuously increases for any l value.

References

[1] G. Guillemot, Ch.-A. Gandin. Analytical model for equiaxed globular solidification in multicomponent alloys. *Acta Materialia*, 97:419–434, 2015.

[2] G. Guillemot, Ch.-A. Gandin. An analytical model with interaction between species for growth and dissolution of precipitates. *Acta Materialia*, 134:375–393, 2017.

[3] G. Guillemot, Ch.-A. Gandin. Corrigendum to 'analytical model for equiaxed globular solidification in multicomponent alloys' [acta mater. 97 (2015) 419-434]. *Acta Materialia*, 122:513–514, 2017.

[4] J. Dantzig, M. Rappaz. *Solidification, 2^{nd} Edition.* EPFL Press, 2016.

[5] W.M. Mullins, R.F. Sekerka. Morphological stability of a particle growing by diffusion or heat flow. *Journal of Applied Physics*, 34:323–329, 1963.

[6] J.S. Wey, J. Estrin. On the growth of secondary nuclei. *AIChE Symposium Series*, 68 (121):74–87, 1972.

[7] J.S. Wey, A.K. Gautesen, J. Estrin. A note on the stability of a growing sphere. *Journal of Crystal Growth*, 19:169–176, 1973.

[8] M.L. Wang, J.S. Wey, J. Estrin. Geometric stability of a spherical nucleus growing due to diffusion and interface kinetics. *Journal of The Chinese Institute of Chemical Engineers*, 7:119–126, 1976.

[9] M.-L. Wang, B. L. Yang. Geometric stability of a cylindrical nucleus growing in a supersaturated solution. *Journal of Chemical Engineering of Japan*, 12 (2):118–124, 1979.

[10] M.-L. Wang, P.-L. Chen. Shape stability of a cylindrical nucleus growing due to diffusion and interface kinetics. *Journal of the Chinese Institute of Engineers*, 3 (1):39–49, 1980.

[11] J. Colin, P.W. Voorhees. Morphological instability of a solid sphere of dilute ternary alloy growing by diffusion from its melt. *Journal of Crystal Growth*, 448:17–20, 2016.

[12] H.-J. Diepers, A. Karma. Theory of growth of spherical precipitates from solid solution. *Solidification processes and microstructures, TMS*, pages 369–371, 2004.

[13] M. Abramowitz, I. Stegun. *Handbook of Mathematical Functions - Tenth printing.* National Institute of Standards and Technology, 1972.

[14] M. I. Tribelsky, S. I. Anisimov. Tuned mullins-sekerka instability: Exact results. *Physical Review E*, 90:042403–1–5, 2014.

[15] TCAL2. TCS Al-Alloys Database, Version v2.1.1, Thermo-Calc Software AB, Stockholm, Sweden, 2013.

[16] MOBAL2. MOBAL2, TCS Al-Alloys Mobility Database v2.0, Thermo-Calc Software AB, Stockholm, Sweden, 2011.

[17] O. Hunziker. Theory of plane front and dendritic growth in multicomponent alloys. *Acta Materialia*, 49:4191–4203, 2001.